Wave spectral shapes in the coastal waters based on measured data off Karwar, west coast of India

Anjali Nair M, Sanil Kumar V

Ocean Engineering Division

Council of Scientific & Industrial Research-National Institute of Oceanography

Dona Paula 403 004, Goa India

*Correspondence to email:sanil@nio.org Tel: 0091 832 2450 327

Abstract

Understanding of the wave spectral shapes is of primary importance for the design of marine facilities. In this paper, the wave spectra collected from January 2011 to December 2015 in the coastal waters of the eastern Arabian Sea using the moored directional waverider buoy are examined to know the temporal variations in the wave spectral shape. Over an annual cycle, for 31.15% of the time, peak frequency is between 0.08 and 0.10 Hz and the significant wave height is also relatively high (~ 1.55 m) for waves in this class. The slope of the high-frequency tail of the monthly average wave spectra is high during the Indian summer monsoon period (June-September) compared to other months and it increases with increase in significant wave height. There is not much interannual variation in slope for swell dominated spectra during the monsoon, while in the non-monsoon period, when wind-seas have much influence, the slope varies significantly. Since the exponent of the high-frequency part of the wave spectrum is within the range from -4 to -3 during the monsoon period, Donelan spectrum shows better fit for the high-frequency part of the wave spectra in monsoon months compared to other months.

Key Words: Ocean surface waves, wind waves, Arabian Sea, wave spectrum, high-frequency tail

1. Introduction

Information on wave spectral shapes are required for designing marine structures (Chakrabarti, 2005) and almost all the wave parameters computations are based on the wave spectral function (Yuan and Huang, 2012). The growth of waves and the correspondent spectral shape is due to the complex ocean-atmosphere interactions, while the physics of air-sea interaction is not completely understood (Cavaleri et al., 2012). The shape of the wave spectrum depends on the factors governing the wave growth and decay, and a number of spectral shapes have been proposed in the past for different sea states (see Chakrabarti, 2005 for a review). The spectral shape is maintained by nonlinear transfer of energy through nonlinear four-wave interactions (quadruplet interactions) and white-capping (Gunson and Symonds, 2014). The momentum flux between the ocean and atmosphere govern the high-frequency wave components (Cavaleri et al., 2012). According to Philips, the equilibrium ranges for low-frequency and high-frequency region is proportional to f^{-5} and f^{-4} (where f is the frequency) respectively. Several field studies made since JONSWAP (Joint North Sea Wave Project) field campaign reveals an analytical form for wave spectra with the spectral tail proportional to f^{-4} (Toba, 1973; Kawai et al., 1977; Kahma, 1981; Forristall, 1981; Donelan et al., 1985). Usually, there is a predominance of swell fields in large oceanic areas, which is due to remote storms (Chen et al., 2002; Hwang et al., 2011; Semedo et al., 2011). The exponent used in the expression for the frequency tail has different values (see Siadatmousavi et al., 2012 for a brief review). For shallow water, Kitaigordskii et al. (1975) suggested f^{-3} tail, Liu (1989) suggested f^{-4} for growing young wind-seas and f^{-3} for fully developed wave spectra. Badulin et al. (2007) suggested f^{-4} for frequencies where nonlinear interactions are dominant. The study carried out at Lake George by Young and Babanin (2006) revealed that in the frequency range $5f_p < f < 10f_p$, the average value of the exponent 'n' of f^{-n} is close to 4. Whereas, some studies in real sea conditions indicate that high-frequency shape of f^{-4} applies up to few times the peak frequency (f_p) and then decays faster with frequency. The spectra for coastlines in Currituck Sound with short fetch condition showed a decay closer to f^{-5} when f is greater than two or three times the peak frequency (Long and Resio, 2007). Gagnaire-Renou et al. (2010) found that the energy input from wind and dissipation due to white-capping have a significant influence on the high-frequency tail of the spectrum.

The physical processes in the north Indian Ocean have a distinct seasonal cycle (Shetye et al., 1985; Ranjha et al., 2015) and the surface wind-wave field is no exception (Sanil Kumar et al., 2012). In the eastern Arabian Sea (AS), significant wave height (H_{m0}) up to 6 m is measured in the monsoon period (June to September), and during rest of the period, H_{m0} is normally less than 1.5 m (Sanil Kumar and Anand, 2004). Sanil Kumar et al. (2014) observed that in the eastern AS, the wave spectral shapes are different at two locations within 350 km distance, even though the difference in the integrated parameter like H_{m0} is marginal. Dora and Sanil Kumar (2015) observed that waves at 7-m water depth in the nearshore zone off Karwar are high energy waves in the monsoon and low to moderate waves in the non-monsoon period (January to May and October to December). Dora and Sanil Kumar (2015) study shows similar contribution of wind-seas and swells during the pre-monsoon (February to May), while swells dominate the wind-sea in the post-monsoon (October to January) and the monsoon period. A study was carried out by Glejin et al. (2012) to find the variation in wave characteristics along the eastern AS and the influence of swells in the nearshore waves at 3 locations during the monsoon period in 2010. This study shows that the percentage of swells in the measured waves was 75 to 79% at the locations with higher percentage of swells in the northern portion of AS compared to that at the southern side. Wind and wave data measured at a few locations along the west coast of India for short-period, one to two months as well as the wave model results were analysed to study the wave characteristics in the deep as well as nearshore regions during different seasons (Vethamony et al., 2013). From the wave data collected for two years period (2011 and 2012) along the eastern AS, the swells of period more than 18 s and significant wave height less than 1 m which occur for 1.4 to 3.6% of the time were separated and their characteristics were studied by Glejin et al. (2016). Anjali Nair and Sanil Kumar (2016) presented the daily, monthly, seasonal and annual variations in the wave spectral characteristics for a location in the eastern AS and reported that over an annual cycle, 29 % of the wave spectra are single-peaked spectra and 71 % are multi-peaked spectra. Recently Amrutha et al. (2017) by analysing the measured wave data in October reported that the high waves (significant wave height > 4 m) generated in an area bounded by 40-60° S and 20-40° E in the south Indian Ocean reached the eastern AS in 5-6 days and resulted in the long-period waves. The earlier studies indicate that the spectral tail of the high-frequency part shows large variation and its variation with seasons are not known. Similarly, the shape of the parametric spectra are also different and hence it is important to identify the spectral shapes based on the measured data covering all the seasons and different years.

The discussion above shows that there is a strong inspiration to study the high-frequency tail of the wave spectrum. For the present study, we used the directional waverider buoy measured wave spectral data at 15-m water depth off Karwar, west coast of India, over 5 years during 2011 to 2015 and evaluated the nearshore wave spectral shapes in different months. This study addresses two main questions: (1) How the high-frequency tail of the wave spectrum varies in different months, and (2) What are the spectral parameters for the best-fit theoretical spectra. This paper is organized as follows: the study area is introduced in section 2, details of data used and methodology in section 3. Section 4 presents the results of the study and the conclusions are given in section 5.

2. Study area

The coastline at Karwar is 24º inclined to the west from the north, and the 20 m depth contour is inclined 29º to the west. Hence, large waves in the nearshore will have an incoming direction close to 241º, since waves get aligned with the depth contour due to refraction. At 10, 30 and 75 km distance from Karwar, the depth contours of 20, 50 and 100 m are present (Fig. 1). The study region is under the seasonally reversing monsoon winds, with winds from the northeast during the post-monsoon and from the southwest during the monsoon period. The monsoon winds are strong and the total seasonal rainfall is 280 cm. The average monthly sea level at Karwar varies from 1.06 m (in September) to 1.3 m (in January) with respect to chart datum and the average tidal range is 1.58 m during spring tides and 0.72 m during neap tides (Sanil Kumar et al., 2012).

3. Data and methods

The waves off Karwar (14° 49’ 56” N and 74° 6’ 4” E) were measured using the directional waverider buoy (DWR-MKIII) . Measurements are carried out from 1 January 2011 to 31 December 2015. The data of heave and two translational motion of the buoy are sampled at 3.84 Hz. A digital high-pass filter with a cut off at 30 s is applied to the 3.84 Hz samples. At the same time it converts the sampling rate to 1.28 Hz and stores the time series data at 1.28 Hz. From the time series data for 200s, the wave spectrum is obtained through a fast Fourier transform (FFT). During half an hour 8 wave spectra of a 200 s data interval each are collected and averaged to get a

representative wave spectrum for half an hour (Datawell, 2009). The wave spectrum is with a resolution of 0.005 Hz from 0.025 Hz to 0.1 Hz and is 0.01 Hz from 0.1 to 0.58 Hz. Bulk wave parameters; significant wave height (H_{m0}) which equals $4\sqrt{m_o}$ and mean wave period (T_{m02}) based on second order moment, which equals $\sqrt{m_0/m_2}$) are obtained from the spectral moments. Where m_n is the n^{th} order spectral moment ($m_n = \int_0^\infty f^n S(f)df$, n=0 and 2), S(f) is the spectral energy density and f is the frequency. The spectral peak period (Tp) is estimated from the wave spectrum and the peak wave direction (Dp) is estimated based on circular moments (Kuik et al., 1988). The wind-seas and swells are separated through the method described by Portilla et al. (2009) and the wind-sea and the swell parameters are computed by integrating over the respective spectral parts. Measurements reported here are in Coordinated Universal Time (UTC), which is 05:30 h behind the local time. U_{10} is the wind speed at 10-m height obtained from reanalysis data of zonal and meridional components at 6 hourly intervals from NCEP / NCAR (Kalnay et.al., 1996) and is used to study the influence of wind speed on the spectral shape.

Since the frequency bins over which the wave spectrum estimated is same in all years, the monthly and seasonally averaged wave spectrum is computed by taking the average of the spectral energy density at the respective frequencies of each spectrum over the specified time.

Wave spectrum continues to develop through non-linear wave-wave interactions even for very long times and distances. Hence, most of the wave spectrum is not fully developed and cannot be represented by Pierson-Moskowitz (PM) spectrum (Pierson and Moskowitz, 1964). Accordingly, an additional factor was added to the PM spectrum in order to improve the fit to the measured spectrum. The JONSWAP spectrum (Hasselmann et al., 1973) is thus a PM spectrum multiplied by an extra peak enhancement factor γ. The high-frequency tail of the JONSWAP spectrum decays in a form proportional to $f^{-5.}$ A number of studies reported that high-frequency decay is by a form proportional to $f^{-4.}$ Modified JONSWAP spectrum including Toba's formulation of saturation range was proposed by Donelan et al. (1985). The JONSWAP and Donelan spectrum used in the study are given in eqns. (1) and (2).

$$S(f) = \frac{\alpha g^2}{(2\pi)^4 f^5} \exp\left[-\frac{5}{4}\left(\frac{f}{f_p}\right)^{-4}\right] \gamma^{\exp\left[-(f-f_p)^2 / 2\sigma^2 f_p\right]} \quad \text{..... (1)}$$

$$S(f) = \frac{\alpha g^2}{(2\pi)^4 f^4 f_p} \exp\left[-\left(\frac{f}{f_p}\right)^{-4}\right] \gamma^{\exp\left[-(f-f_p)^2 / 2\sigma^2 f_p^2\right]} \quad \text{.....(2)}$$

Where γ is the peak enhancement parameter; α is Philip's constant; f is the wave frequency; g is the gravitational acceleration and σ is the width parameter.

$$\sigma = \begin{cases} 0.07, & f < f_p \\ 0.09, & f \geq f_p \end{cases}$$

An exponential curve $y = k.f^b$ is fitted for high-frequency part of the spectrum and the exponent (value of b) is estimated for the best fitting curve based on statistical measures such as least square error and bias. The slope of the high-frequency part of the wave spectrum is represented by the exponent of the high-frequency tail.

For the present study, JONSWAP spectrum is tested by fitting for the whole frequency range of the measured wave spectrum. It is found out that the JONSWAP spectra do not show a good fit for higher frequency range, whereas Donelan spectrum shows better fit for the high-frequency range. Hence, JONSWAP spectrum is used for the lower frequency range up to spectral peak and Donelan spectrum is used for the higher frequency range from the spectral peak for single-peaked wave spectrum. Theoretical wave spectra are not fitted to the double-peaked wave spectra.

4. Results and discussions

4.1 Bulk wave parameters

Mostly the wave conditions (~ 75%) at the buoy location are intermediate and shallow-water waves (where water depth is less than half the wavelength, d < L/2), this condition is not satisfied during ~ 25% of the time due to waves with mean periods of 4.4 s or less. This study, therefore, deals with shallow, intermediate and deepwater wave climatology. Hence, bathymetry will significantly influence the wave characteristics.

182 The persistent monsoon winds generate choppy seas with average wave heights of 2 m and
183 mean wave period of 6.5 s. Fig. 2 shows that in the monsoon, the observed waves had a maximum
184 H_{m0} of about 5 m, with H_{m0} of 2-2.5 m more common during this period. The maximum H_{m0}
185 measured during the study period is on 21 June 2015 17:30 UTC (Fig. 2a). Mean wave periods
186 (T_{m02}) at the measurement location ranged from 4-8 s (Fig. 2b). Wave direction during monsoon is
187 predominantly from the west due to refraction towards the coast. The fluctuation in H_{mo} due to the
188 southwest monsoon is seen in all the years (Fig. 2a). High waves (H_{m0} > 2 m) during 27-29
189 November 2011 are due to the deep depression ARB04 formed in the AS. During the study period,
190 the annual average H_{m0} is same (~1.1 m) in all the years (Table 1). In 2013, the data during August
191 could not be collected and hence resulted in lower annual average H_{m0}. Over the 5 years, small
192 waves (H_{m0} < 1 m) account for a large proportion (63.94%) of measured data and only during
193 0.16% of the time, H_{m0} exceeded 4 m (Table 2). The 25th and 75th percentiles of the H_{m0} distribution
194 over the entire analysis period are 0.6 and 1.4 m.
195
196 Waves with low heights (H_{m0} < 1 m) are with the mean period in a large range (2.7-10.5 s),
197 whereas high waves (H_{m0} > 3m) have mean wave period in a narrow range (6.1-9.3 s) (Table 2).
198 For waves with H_{m0} higher than 3 m, the Tp never exceeded 14.3 s and for waves with H_{m0} less
199 than 1 m, Tp up to 22.2 s are observed (Fig. 2c) and the long period swells (14-20 s) are with H_{m0} <
200 2.5 m. Around 7% of the time during 2011-2015, waves have peak period more than 16.7 s (Table
201 3). Peak frequencies between 0.08 and 0.10 Hz, equivalent to a peak wave period of 10 - 12.5 s are
202 observed 31.15% of the time and the H_{m0} is also relatively high (~ 1.55 m) for waves in this class.
203 During the annual cycle, the wave climate is dominated by low (0.5 > H_{m0} >1m) intermediate-
204 period (Tp ~10-16s) south-westerly swell. Waves from the northwest are with Tp less than 8 s (Fig.
205 3).
206
207 The wave roses during 2011-2015 indicate that around 38% of the time during the period
208 2011 to 2015, the predominant wave direction is SSW (225°) with long period (14 - 18s) and
209 intermediate period (10 - 14s) waves (Fig. 3). A small percentage of long-period waves having H_{m0}
210 more than 1m are observed from the same direction in which more than 80% are swells (Fig. 3c).
211 Intermediate period waves observed having H_{m0} less than 1m, contain 20 - 60% of swells. Around
212 10-15% of the waves observed during the period are from the west, which includes intermediate
213 and short period waves with H_{m0} varying from 1.5 to 3m. These intermediate period waves from

west having H_{m0} between 2.5 - 3m contain more than 80% of swells. Waves from NW are short period waves with H_{m0} between 0.5 and 1.5; in which swell percentage is very less showing the influence of wind-sea (Fig. 3d). High waves observed in the study area consists of more than 80% swells.

Date versus year plots of significant wave height (Fig. 4) shows that H_{m0} has its maximum values (H_{m0} >3m) during the monsoon period with a wave direction of WSW and peak wave period of 10 - 12s (intermediate period). The mean wave period shows its maximum values (6 - 8s) during the monsoon period. During January–May in all the years, H_{m0} is low (H_{m0} < 1m) with waves from SW, W and NW directions. NW waves observed are the result of strong sea breezes existing during this period. Both long-period (Tp > 14s), intermediate-period (10 < Tp <14s) and short-period (Tp < 8s) waves are observed during this period and hence, the mean wave period observed is low compared to the monsoon (Fig. 4d). During October to December, similar to the pre-monsoon period, H_{m0} observed is less than 1m, but the wave direction is predominantly from SW and W, with least NW waves. Short period waves are almost absent during this period, and the condition is similar for all the years. The interannual variations in H_{m0} are less than 15% (Fig. 4). Primary seasonal variability in waves is due to the monsoonal wind reversal. During January-March, there is a shift in the occurrences of northwest swells.

4.2 Wave spectrum

Normalisation of the wave spectrum is done to know the spread of energy in different frequencies. Since the range of maximum spectral energy density in a year is large (~ 60 m^2/Hz), each wave spectrum is normalised through dividing the spectral energy density by the maximum spectral energy density of that spectrum. The normalized wave spectral energy density contours are presented for different years to know the wind-sea/swell predominance (Fig. 5). The predominance of both the wind-seas and swells are observed in the non-monsoon period, whereas in the monsoon only swells are predominant (Fig. 5). The separation of swells and wind-seas indicates that over an annual cycle, around 54% of the waves are swells. Glejin et al. (2012) reported that the dominance of swells during monsoon is due to the fact that even though the wind at the study region is strong during monsoon, the wind over the entire AS also will be strong and when these swells are added to the wave system at the buoy location, the energy of the swell increases (Donelan, 1987) and will result in dominance of swells. The spread of spectral energy to higher frequencies (0.15 to 0.25 Hz)

247 is predominant during January-May (Fig. 5) due to sea-breeze in the pre-monsoon period (Neetu et
248 al., 2006; Dora and Sanil Kumar, 2015). In the monsoon during the wave growth period, the
249 spectral peak shifts from 0.12-0.13 Hz to 0.07-0.09 Hz (lower frequencies).
250
251 An interesting phenomenon is that the long-period (> 18 s) swells are present for 2.5% of
252 the time during the study period. The buoy location at 15 m water depth is exposed to waves from
253 northwest to south with the nearest landmass at ~ 1500 km in the northwest (Asia), ~ 2500 km in
254 the west (Africa), ~ 4000 km in the southwest (Africa) and ~ 9000 km in the south (Antarctica)
255 (Amrutha et al., 2017). Due to its exposure to the Southern Oceans and the large fetch available,
256 swells are present all year round in the study area and the swells are dominant in the non-monsoon
257 (Glejin et al., 2013). Throughout the year, waves with period more than 10 s (low-frequency < 0.1
258 Hz waves) are the southwest swells whereas with seasons the direction of short-period waves
259 changes (Fig. 5). Amrutha et al. (2017) reported that the long-period waves observed in the eastern
260 AS are the swells generated in the south Indian Ocean. In the monsoon season, the waves with
261 high-frequency are predominantly from west-southwest, whereas in the non-monsoon they are from
262 the northwest. In the non-monsoon period, the predominance of wind-seas and swells fluctuated
263 and hence the mean wave direction also changed frequently (Fig. 5). The average direction of
264 waves with H_{m0} < 1m shows the northwest wind-seas and the southwest swells, whereas, for high
265 waves (H_{m0} > 3m), the difference between the swell and wind-sea direction decreases. This is
266 because the high waves get aligned to the bottom contour before 15 m water depth on its approach
267 to the shallow water.
268
269 The interannual changes of wave spectral energy density for different months in the period
270 2011-2015 are studied by computing the monthly average wave spectra for all the years (Fig. 6). In
271 the non-monsoon period, the wave spectra observed is double-peaked, indicating the presence of
272 wind-seas and swells, whereas during the monsoon, due to the strong southwest winds, single
273 peaked spectrum is observed, i.e. the swell peak with low-frequency and high spectral energy
274 density. Along the Indian coast, Harish and Baba (1986), Rao and Baba (1996) and Sanil Kumar et
275 al. (2003) found out that wave spectra are generally multipeaked and that the double peaked wave
276 spectra are more frequent during low-sea states (Sanil Kumar et al., 2004). Sanil Kumar et al.
277 (2014), Sanil Kumar and Anjali (2015) and Anjali and Sanil Kumar (2016) have also observed that
278 double-peaked spectrum in the monsoon period in the eastern AS are due to the locally generated

279 wind-seas and the south Indian Ocean swells. In the study area, from January to May and October
280 to December, the swell peak is between the frequencies 0.07 and 0.08 Hz (12.5 < Tp < 14.3s), but
281 in the monsoon period, the swell peak is around 0.10 Hz, in all the years studied. This shows long-
282 period swells (Tp > 13s) in the non-monsoon period and intermediate period swells (8 < Tp <13s)
283 in the monsoon. Glejin et al. (2016), also observed the presence of low-amplitude long-period
284 waves in the eastern AS in the non-monsoon period and intermediate period waves in the monsoon
285 period. This is because of the propagation of swells from the southern hemisphere is more visible
286 during the non-monsoon period due to the calm conditions (low wind-seas) prevailing in the eastern
287 AS. Whereas during the monsoon period, these swells are less due to the turbulence in the north
288 Indian Ocean (Glejin et al., 2013). Large interannual variations are observed for monthly average
289 wave spectrum in all months except in July. This is because July is known to be the roughest month
290 over the entire annual cycle and southwest monsoon reaches its peak during July. Hence, the
291 influence of temporally varying wind-seas on the wave spectrum is least during July compared to
292 other months. Due to the early onset (on 1 June) and advancement of monsoon during 2013
293 compared to other years, the monthly average value of the maximum spectral energy is observed in
294 June 2013 (Fig. 6). The wave spectra of November 2011 is distinct from that of other years, with
295 low wind-sea peak frequency, i.e. 0.13 Hz due to the deep depression ARB04, occurred south of
296 India near Cape Comorin, during 26 November–1 December, with a sustained wind speed of 55
297 km/h. During October 2014, the second peak is observed at 0.11 Hz with comparatively high
298 energy showing the influence of cyclonic storm NILOFAR. It is an extremely severe cyclonic
299 storm that occurred during the period 25-31 October 2014, originated from a low-pressure area
300 between Indian and Arabian Peninsula, with the highest wind speed of 215 km/h and affected the
301 areas of India, Pakistan and Oman. Significant interannual variation is observed in the wind-sea
302 peak frequency. Wave spectra averaged over each season (Fig. 7) shows that the interannual
303 variations in energy spectra averaged over full year period almost follows the pattern of wave
304 spectra averaged over monsoon period, indicating the strong influence of monsoon winds over the
305 wave energy spectra in the study area. Interannual variations within the spectrum are more for
306 wind-sea region compared to swell region. During the study period, the maximum spectral energy
307 observed is during 2011 monsoon.
308
309 For different frequencies, the monthly average wave direction is shown in Fig. 8. It is
310 observed that throughout the year the mean wave direction of the swell peak is southwest (200-

311 250^{o}). In the non-monsoon period, the wind-sea direction is northwest (280-300°), except in
312 October and November. This is due to the wind-seas produced by sea breeze which has the
313 maximum intensity during the pre–monsoon season. Interannual variability in wave direction is
314 highest during October and November, where the wind-seas from southwest direction are also
315 observed. This is because, during these months, the wind speed and the strength of the monsoon
316 swell decreases, which makes the low energy wind-seas produced by the withdrawing monsoon
317 winds more visible.
318
319 Contour plots of spectral energy density (normalized) clearly show the predominance of
320 wind-seas and swells during the non-monsoon period (Fig. 9). In the monsoon period, the spectral
321 energy density is mainly confined to a narrow frequency range (0.07-0.14 Hz) and the wave spectra
322 are mainly single peaked with maximum energy within the frequency range 0.08-0.10 Hz, having
323 direction 240^{o}. Glejin et al. (2012) reported that in the monsoon season, the spectral peak is
324 between 0.08 and 0.10 Hz (12-10s) for ~ 72% of the time in the eastern AS. Earlier studies also
325 reported dominance of swells in the eastern AS during the monsoon (Sanil Kumar et al., 2012;
326 Glejin et al., 2012). Above 0.15 Hz, energy gradually decreases, with the lowest energy observed
327 between 0.30 and 0.50 Hz. Wind-sea energy is comparatively low during October, November and
328 December and occurs mostly in the frequency range less than 0.20 Hz, whereas, during January-
329 May, the frequency exceeds 0.20 Hz. In the pre-monsoon period, wind-sea plays a major role in
330 nearshore wave environment (Rao and Baba, 1996). Wind-sea energy is found to be low during
331 April 2015 (Fig. 6), because of reduction in local winds. The occurrence of wind-seas is very less
332 during most of the time in November except during 2011, due to the deep depression ARB04.
333 .
334 The behavior of the high-frequency part of the spectrum is governed by the energy balance
335 of waves generated by the local wind fields. When the wind blows over a long fetch or for a long
336 time, the wave energy for a given frequency reaches the equilibrium range and the energy input
337 from the wind is balanced by energy loss to lower frequencies and by wave breaking (Torsethaugen
338 and Haver, 2004). The high-frequency tail slope of the monthly average wave spectrum in different
339 years shows that the slope is high ($b < -3.1$), during June to September and the case is same for all
340 the years studied (Table 4). During all other months, the exponent in the expression for the
341 frequency tail is within the range - 3.1 to -1.5. The distribution of exponent values for different
342 significant wave height ranges shows that the slope increases (exponent decrease from -2.44 to -

4.20) as the significant wave height increases and reaches a saturation range. For frequencies from 0.23 to 0.58 Hz in the eastern AS during January-May, Amrutha et al. (2017) observed that the high-frequency tail has $f^{-2.5}$ pattern at 15 m water depth and for frequencies ranging from 0.31 to 0.55 Hz, the high-frequency tail follows f^{-3} at 5 m water depth. Since H_{mo} is maximum during the monsoon period, the slope is also maximum during June to September. There is no much interannual variation in slope for swell dominated spectra during the monsoon, while in the non-monsoon period when wind-seas have much influence, the slope varies significantly.

The most obvious manifestations of nonlinearity are sharpening of the wave crests and the flattening of the wave troughs and these effects are reflected in the skewness of the sea surface elevation (Toffoli, 2006). Zero skewness indicates linear sea states, positive skewness value indicate that the wave crests are bigger than the troughs. Figure 10 shows that nonlinearity increases with increase in H_{m0}. The slope of the high-frequency end of the wave spectrum becomes steeper when the wave nonlinearity increases. Donelan et al. (2012) find that in addition to the k^{-4} dissipation that swells modulate the equilibrium in breaking waves dependent on the mean surface slope, while Melville (1994) also quantified a relation between wave packet slopes and dissipation rate. These results are specific to breaking waves, but one might expect similar relations between surface dynamics and dissipation rate for non breaking waves. A function of the form: $A * \exp(\lambda H_{m0}) + s0$, with initial parameters of $A = 8$, $\lambda = -2.4$, $s0 = -3.7$ is found to fit the exponent of the high-frequency tail data with the significant wave height (Fig. 11a). The functional representation of the exponent of the high-frequency tail data with H_{m0} shown in Fig. 11a might be useful in revealing the physical connection, and at the very least would provide a predictive basis relating spectral slopes with mean significant wave heights as a basis for future research. It is shown in Fig. 11b that the exponent decreases (slope increases) as the mean wave period increases. The study shows that the tail of the spectrum is influenced by the local wind conditions (Fig. 11c) and the influence is more with the zonal component (u) of the wind than on the meridional component (v) (Figs. 11e and 11f). The exponent of the high-frequency tail decreases with the increase of the inverse wave age (U_{10}/c), where c is the celerity of the wave.

4.3 Comparison with theoretical wave spectra

In the monsoon period, the spectrum is single peaked with high spectral energy density and during this period JONSWAP spectrum is fitted up to the peak frequency and after that Donelan spectrum is used. The monthly average wave spectra during the monsoon period for the year 2011, is compared with JONSWAP and Donelan theoretical wave spectra in Figure 12. It is found that JONSWAP and Donelan spectra with modified parameters describe well the wave spectra at low frequencies and high frequencies respectively. The values for α and Υ were randomly varied within a range to find out the values for which, the theoretical spectrum best fits the measured spectrum and those values were used to plot the theoretical spectrum. The values of α and Υ thus obtained, for June, July, August and September are given in Table 6. From the table, the average values of α and Υ, for the monsoon months are obtained as 0.0009 and 1.82 for JONSWAP spectra and 0.0274 and 1.64 for Donelan spectra respectively. These values are less than the generally recommended values of α and Υ; 0.0081 and 3.3. α is a constant that is related to the wind speed and fetch length. For all the data, Donelan spectrum fitted is proportional to f^{n}, where n is the exponent value of the high-frequency tail. The theoretical spectrum JONSWAP and Donelan cannot completely describe the high-frequency tail of the measured spectrum since the high-frequency tail in these spectrum decays in the form of f^{-5} and f^{-4} respectively. Since the exponent of the high-frequency tail of the wave spectrum is within the range -4 to -3 during the monsoon period, Donelan spectrum shows better fit for monsoon spectra compared to other months (Fig. 11).

5. Concluding remarks

In this paper, the variations in the wave spectral shapes in different months for a nearshore location are investigated, based on in situ wave data obtained from a moored directional waverider buoy. Interannual variations within the spectrum are more for wind-seas compared to swells. The maximum significant wave height measured at 15 m water depth is 5 m and the annual average H_{m0} has similar value (~1.1 m) in all the years. Over the 5 years, small waves ($H_{m0} < 1$ m) account for a large proportion of measured data (63.94% of the time). The study shows that high waves ($H_{m0} > 2$ m) are with spectral peak period between 8 and 14 s and the long period swells (14-20 s) are with $H_{m0} < 2.5$ m. The high-frequency slope of the wave spectrum (the exponent decreases from -2.44 to -4.20) increases with increase in significant wave height and mean wave period. During the monsoon period, Donelan spectrum shows better fit for monsoon spectra compared to other months

since the exponent of the high-frequency part of the wave spectrum is within the range -4 to -3. The decay of the high-frequency waves are fastest with depth and hence, the high-frequency tail values observed in the study will be different for different water depths.

Acknowledgments

The authors acknowledge the Earth System Science Organization, Ministry of Earth Sciences, New Delhi for providing the financial support to conduct part of this research. We thank TM Balakrishnan Nair, Head OSISG and Arun Nherakkol, Scientist, INCOIS, Hyderabad and Jai Singh, Technical Assistant, CSIR-NIO for the help during the collection of data. We thank Dr. Bhat and Dr. J L Rathod, Department of Marine Biology, Karnataka University PG Centre, Karwar for providing the logistics required for wave data collection. This work contributes part of the Ph.D. work of the first author. This paper is dedicated to the memory of our esteemed colleague Ashok Kumar, in recognition of his substantial contributions in initiating the long-term wave measurements in the shallow waters around India. We thank the topic editor and both the reviewers for their critical comments and the suggestions which improved the scientific content of the publication. This publication is a NIO contribution.

References

Amrutha, M.M., Sanil Kumar, V., and George, J.: Observations of long-period waves in the nearshore waters of central west coast of India during the fall inter-monsoon period, Ocean Engineering, 131, 244-262, 10.1016/j.oceaneng.2017.01.014, 2017.

Anjali, N.M., and Sanil Kumar, V.: Spectral wave climatology off Ratnagiri - northeast Arabian Sea, Natural Hazards, 82, 1565-1588, 2016.

Badulin, S.I., Babanin, A.V., Zakharov, V.E. and Resio, D.: Weakly turbulent laws of wind-wave growth, Journal of Fluid Mechanics., 591, 339-378, 2007.

Cavaleri, L., Fox-Kemper, B., and Hemer, M.: Wind-waves in the coupled climate sys- tem. Bull. Am. Meteorol. Soc., 93, 1651–1661, 2012.

Chakrabarti, S.K.: Handbook of Offshore Engineering, Vol-1, Ocean Engineering Series, Elsevier, p 661, 2005.

436 Chen, G., Chapron, B., Ezraty, R., and Vandemark, D.: A global view of swell and wind-sea
437 climate in the ocean by satellite altimeter and scatterometer. J. Atmospheric and Oceanic
438 Technology., 19(11), 1849-1859, 2002.

439 Datawell.: Datawell Waverider Reference Manual. Datawell BV oceanographic instruments, The
440 Netherlands, Oct. 10, pp.123, 2009.

441 Donelan, M. A.: The effect of swell on the growth of wind waves, Johns Hopkins APL Technical
442 Digest., 8 (1), 18-23, 1987.

443 Donelan, M., Hamilton, H., and Hui, W.H.: Directional spectra of wind-generated waves,
444 Philosophical Transactions of the Royal Society of London A: Mathematical, Physical and
445 Engineering Sciences., 315(1534), 509-562, 1985.

446 Donelan, M.A., Curcic, M., Chen, S.S. and Magnusson, A.K.: Modeling waves and wind stress,
447 Journal of Geophysical Research: Oceans., 117(C11), 2012.

448 Dora, G.U., and Sanil Kumar, V.: Sea state observation in island-sheltered nearshore zone based on
449 in situ intermediate-water wave measurements and NCEP/CFSR wind data, Ocean Dynamics., 65,
450 647-663, 2015.

451 Forristall, G.Z.: Measurements of a saturated range in ocean wave spectra, Journal of Geophysical
452 Research: Oceans., 86(C9), 8075-8084, 1981.Gagnaire-Renou, E., Benoit, M. and Forget, P.: Ocean
453 wave spectrum properties as derived from quasi-exact computations of nonlinear wave-wave
454 interactions, Journal of Geophysical Research: Oceans., 115(C12), 2010.

455 Glejin, J., Sanil Kumar, V., Balakrishnan Nair, T. M., and Singh, J.: Influence of winds on
456 temporally varying short and long period gravity waves in the near shore regions of the eastern
457 Arabian Sea, Ocean Sci., 9, 343–353, doi:10.5194/os-9-343-2013, 2013.

458 Glejin, J., Sanil Kumar, V., Sajiv, P.C., Singh, J., Pednekar, P., Ashok Kumar, K., Dora, G.U., and
459 Gowthaman, R.: Variations in swells along eastern Arabian Sea during the summer monsoon, Open
460 J. Mar. Sci., 2 (2), 43–50, 2012.

461 Glejin, J., Sanil Kumar, V., Amrutha, M.M. and Singh J.:Characteristics of long-period swells
462 measured in the in the near shore regions of eastern Arabian Sea, Int. J. Naval Architecture and
463 Ocean Engineering, 8, 312-319, 2016.

464 Gunson, J., and Symonds, G.: Spectral Evolution of Nearshore Wave Energy during a Sea-Breeze
465 Cycle, J. Phys. Oceanogr., 44(12), 3195-3208, 2014.

466 Harish, C. M., and Baba, M.: On spectral and statistical characteristics of shallow water waves,
467 Ocean Eng., 13(3), 239-248, 1986.

468 Hasselmann, K., Barnett, T.P., Bouws, F., Carlson, H., Cartwright, D.E., Enke, K., Ewing J.A.,
469 Gienapp, H., Hasselmann, D.E., Krusemann, P., Meerburg, A., Muller, P., Olbers, D.J., Richter, K.,
470 Sell, W., and Walden, H.: Measurements of wind-wave growth and swell decay during the Joint
471 North Sea Wave Project (JONSWAP), Deutches Hydrographisches Institut., A8 (12), 95, 1973.

472 Hwang, P.A., Garcia-Nava, H., and Ocampo-Torres, F.J.: Dimensionally Consistent Similarity
473 Relation of Ocean Surface Friction Coefficient in Mixed Seas, J. Phys. Oceanogr 41., 1227–1238.
474 2011.

475 Kahma, K.K.: A study of the growth of the wave spectrum with fetch, Journal of Physical
476 Oceanography., 11(11), 1503-1515, 1981.

477 Kalnay, E., Kanamitsu, M., Kistler, R., Collins, W., Deaven, D., Gandin, L., Iredell, M., Saha, S.,
478 White, G., Woollen, J. and Zhu, Y.: The NCEP/NCAR 40-year reanalysis project, Bulletin of the
479 American meteorological Society., 77(3), 437-471, 1996.

480 Kawai, S., Okada, K. and Toba, Y.: Field data support of three-seconds power law andgu* σ− 4-
481 spectral form for growing wind waves, Journal of Oceanography., 33(3), 137-150, 1977.

482 Kitaigordskii, S.A., Krasitskii, V.P. and Zaslavskii, M.M.: On Phillips' theory of equilibrium range
483 in the spectra of wind-generated gravity waves, Journal of Physical Oceanography., 5(3), 410-420,
484 1975.

485 Kuik, A. J., Vledder, G., and Holthuijsen, L.H.: A method for the routine analysis of pitch and roll
486 buoy wave data, J. Phys. Oceanogr., 18, 1020–1034, 1988.

Liu, A.K., Jackson, F.C., Walsh, E.J. and Peng, C.Y.: A case study of wave-current interaction near an oceanic front, Journal of Geophysical Research: Oceans., 94(C11), 16189-16200, 1989.

Long, C.E. and Resio, D.T.: Wind wave spectral observations in currituck sound, north Carolina, Journal of Geophysical Research: Oceans., 112(C5), 2007.

Longuet-Higgins, M.S.: On the joint distribution of the periods and amplitudes of sea waves, J. Geophys. Res.-Oceans., 80, 2688–2694, 1975.

Neetu, S., Shetye Satish., and Chandramohan, P.: Impact of sea breeze on wind-seas off Goa, west coast of India, Journal Earth System Science., 115, 229-234, 2006.

Pierson, W.J., and Moskowitz, L.: A proposed form for fully developed seas based on the similarity theory of S.A.Kitaigorodski, J. Geophys. Res.-Oceans., 69(24), 5181-5190, 1964.

Portilla, J., Ocampo-Torres, F.J., and Monbaliu, J.: Spectral Partitioning and Identification of Wind-sea and Swell, J. Atmospheric and Oceanic Technology., 26, 117-122, 2009.

Ranjha, R., Tjernström, M., Semedo, A., Svensson, G.: Structure and variability of the Oman Coastal Low-Level Jet, Tellus A, 67, 25285, http://dx.doi.org/10.3402/tellusa.v67.2528 , 2015.

Rao, C. P., and Baba, M.: Observed wave characteristics during growth and decay: a case study, Continental Shelf Res., 16(12), 1509-1520, 1996.

Sanilkumar, V., Ashokkumar, K. and Raju, N.S.N.: Wave characteristics off Visakhapatnam coast during a cyclone, Indian Academy of Sciences., 2004.

Sanil Kumar, V., Johnson, G., Dora, G.U., Chempalayil, S.P., Singh, J., and Pednekar, P.: Variations in nearshore waves along Karnataka, west coast of India, J. Earth Systems Science., 121, 393-403, 2012.

Sanil Kumar, V., Anand, N.M., Kumar, K.A., and Mandal, S.: Multipeakedness and groupiness of shallow water waves along Indian coast, J. Coastal Res., 19, 1052-1065, 2003.

Sanil Kumar, V., and Anand, N.M.: Variation in wave direction estimated using first and second order Fourier coefficients, Ocean Eng., 31, 2105–2119, 2004.

512 Sanil Kumar, V. and Anjali Nair, M.: Inter-annual variations in wave spectral characteristics at a
513 location off the central west coast of India, Ann. Geophys., 33, 159–167, doi:10.5194/angeo-33-
514 159-2015, 2015.

515 Sanil Kumar, V., Shanas, P.R., and Dubhashi, K.K.: Shallow water wave spectral characteristics
516 along the eastern Arabian Sea, Natural Hazards, 70, 377–394, 2014.

517 Semedo, A., Sušelj, K., Rutgersson, A., and Sterl, A.: A global view on the wind-sea and swell
518 climate and variability from ERA-40, J. Climate, 24(5), 1461-1479, 2011.

519 Shetye, S.R., Shenoi, S.S.C., Antony, A.K., and Kumar, V.K.: Monthly-mean wind stress along the
520 coast of the north Indian Ocean, J. Earth Syst. Sci., 94, 129–137, doi:10.1007/BF02871945, 1985.

521 Shore Protection Manual., U.S. Army Coastal Engineering Research Center, Department of the
522 Army, Corps of Engineers, U.S. Govt. Printing Office, Washington, DC, USA, vols. 1 and 2, 1984.

523 Siadatmousavi, S.M., Jose, F. and Stone, G.W.: On the importance of high frequency tail in third
524 generation wave models, Coastal Engineering., 60, 248-260, 2012.

525 Toba, Y.: Local balance in the air-sea boundary processes, Journal of Oceanography., 29(5), 209-
526 220, 1973.

527 Toffoli, A., Onorato, M. and Monbaliu, J.: Wave statistics in unimodal and bimodal seas from a
528 second-order model, European Journal of Mechanics B/Fluids, 25, 649–661, 2006.

529 Torsethaugen, K., and Haver, S.: Simplified double peak spectral model for ocean waves, In:
530 Proceeding of the 14th International Offshore and Polar Engineering Conference, 2004.

531 Vethamony, P., Rashmi, R., Samiksha, S.V. and Aboobacker, M.: Recent Studies on Wind Seas
532 and Swells in the Indian Ocean: A Review, International J. Ocean and Climate Systems, 4, 63 - 73,
533 2013.

534 Young, I.R. and Babanin, A.V.: Spectral distribution of energy dissipation of wind-generated
535 waves due to dominant wave breaking, Journal of Physical Oceanography., 36(3), 376-394, 2006.

536 Yuan, Y., and Huang, N.E.: A reappraisal of ocean wave studies, J. Geophys. Res.-Oceans.,
537 117(C11), 2012.

538 **Figure captions**

539 Figure 1. Study area along with the wave measurement location in eastern Arabian Sea

540 Figure 2. Time series plot of a) significant wave height, b) mean wave period, c) peak wave period
541 and d) mean wave direction from 1 January 2011 to 31 December 2015. Thick blue line indicates
542 the monthly average values

543 Figure 3. Wave roses during 2011-2015 (a) significant wave height and mean wave direction, (b)
544 peak wave period and mean wave direction, (c) percentage of swell, (d) percentage of wind-sea and
545 mean wave direction

546 Figure 4. Date verses year plot of a) significant wave height b) mean wave direction, c) peak wave
547 period and d) mean wave period

548 Figure 5. Temporal variation of normalized spectral energy density (top panel) and mean wave
549 direction (bottom panel) with frequency in different years

550 Figure 6. Monthly average wave spectra in 2011 to 2015

551 Figure 7. Wave spectra averaged over a) pre-monsoon (February-May), b) monsoon (June-
552 September), c) post-monsoon (October-January) and d) full year in different years

553 Figure 8. Monthly average wave direction at different frequencies in different months

554 Figure 9. Temporal variation of normalized spectral energy density in different months (data from
555 2011 to 2015 used)

556 Figure 10. Scatter plot of significant wave height with skewness of the sea surface elevation in
557 different years

558 Figure 11. Plot of exponent of the high-frequency tail with a) significant wave height, b) mean
559 wave period, c) wind speed, d) inverse wave age, e) u-wind and f) v-wind

560 Figure 12. Fitted theoretical spectra along with the monthly average wave spectra for different
561 month

562

563 Table 1. Number of data used in the study in different years along with range of significant wave
564 height and average value
565

Year	Significant wave height (m)		Number of data	%of data
	Range	Average		
2011	0.3-4.4	1.1	17517	99.98
2012	0.3-3.7	1.1	17323	98.61
2013	0.3-3.6	0.9*	14531	82.94
2014	0.3-4.5	1.1	17284	98.65
2015	0.3-5.0	1.1	14772	84.32

566 * average value is estimated excluding the July month data
567
568
569
570
571
572
573 Table 2. Characteristics of waves in different range of significant wave height
574

Significant wave height range	Number (percentage)	Range of Tp (s)	Mean Tp (s)	Range of T_{m02} (s)	Mean T_{m02} (s)
$H_{m0} < 1$ m	52062 (63.94)	2.6-22.2	12.2	2.7-10.5	4.9
$1 \leq H_{m0} < 2$ m	18297 (22.47)	3.6-22.2	10.5	3.4-10.7	5.7
$2 \leq H_{m0} < 3$ m	9839 (12.08)	6.2-18.0	10.8	5.0-8.9	6.5
$3 \leq H_{m0} < 4$ m	1096 (1.35)	10.0-14.3	11.8	6.1-9.1	7.2
$4 \text{ m} \leq H_{m0}$	133 (0.16)	10.5-14.3	12.6	7.2-9.3	7.8

575
576
577
578
579
580
581 Table 3. Average wave parameters and number of data in different spectral peak frequencies
582

Frequency (f_p) range (Hz)	Number of data and %	H_{m0} (m)	T_{m02} (s)	Peak wave period (s)
$0.04 < f_p \leq 0.05$	318 (0.39)	0.73	5.24	20.19
$0.05 < f_p \leq 0.06$	5341 (6.56)	0.82	5.48	17.16
$0.06 < f_p \leq 0.07$	14764 (18.13)	0.75	5.22	14.73
$0.07 < f_p \leq 0.08$	18221 (22.38)	0.80	5.05	12.96
$0.08 < f_p \leq 0.10$	25364 (31.15)	1.55	5.76	10.88
$0.10 < f_p \leq 0.15$	9459 (11.62)	1.25	5.35	8.07
$0.15 < f_p \leq 0.20$	6355 (7.80)	0.76	4.43	5.72
$0.20 < f_p \leq 0.30$	1487 (1.83)	0.78	3.86	4.36
$0.30 < f_p \leq 0.50$	118 (0.14)	0.66	3.22	3.09

583

584
585 Table 4. Exponent of the high-frequency tail of the monthly average wave spectra in different
586 years
587

Months	Exponent of the high-frequency tail					
	2011	2012	2013	2014	2015	2011-2015
January	-2.08	-2.93	-2.97	-2.72	-2.81	-2.72
February	-2.41	-3.02	-2.74	-2.99	-3.06	-2.85
March	-2.75	-2.91	-2.82	-2.76	No data	-2.81
April	-2.56	-2.74	-2.64	-2.71	-2.19	-2.60
May	-2.59	-2.67	-2.63	-2.42	-2.51	-2.56
June	-3.64	-3.53	-3.55	-3.82	-3.58	-3.55
July	-3.76	-3.55	No data	-3.82	-3.63	-3.70
August	-3.63	-3.58	-3.40	-3.52	-3.65	-3.58
September	-3.41	-3.44	-3.16	-3.38	-3.00	-3.30
October	-2.02	-2.77	-3.03	-2.52	-2.61	-2.68
November	-1.78	-2.43	-1.77	-1.55	-1.65	-1.84
December	-1.69	-2.23	-1.95	-2.06	-1.79	-1.94

588
589
590
591
592
593
594
595 Table 5. Exponent of the high-frequency tail of the average wave spectra in different wave height
596 ranges
597

Range of H_{m0} (m)	Exponent of the high-frequency tail
0-1	-2.44
1-2	-3.26
2-3	-3.67
3-4	-4.21
4-5	-4.21

598
599

600 Table 6. Parameters of the fitted wave spectrum in different years
601
602

Year		JONSWAP spectrum		Donelan spectrum	
		α	ϒ	α	ϒ
2011	June	0.0013	2.2	0.0028	2.0
	July	0.0016	1.5	0.0021	1.7
	August	0.0013	1.8	0.0029	1.7
	September	0.0004	2.3	0.0021	1.6
2012	June	0.0015	1.6	0.0029	2.0
	July	0.0010	2.1	0.0031	1.9
	August	0.0009	2.2	0.0032	1.7
	September	0.0006	2.0	0.0024	1.8
2013	June	0.0006	3.3	0.0030	1.9
	July	No data			
	August	0.0012	1.1	0.0038	1.4
	September	0.0005	1.9	0.0042	1.4
2014	June	0.0010	1.1	0.0010	1.6
	July	0.0006	2.5	0.0019	1.2
	August	0.0006	1.5	0.0021	1.2
	September	0.0011	1.1	0.0032	1.4
2015	June	0.0011	1.4	0.0023	1.8
	July	0.0011	1.9	0.0024	1.8
	August	0.0008	1.8	0.0024	1.4
	September	0.0006	1.3	0.0043	1.6

603
604

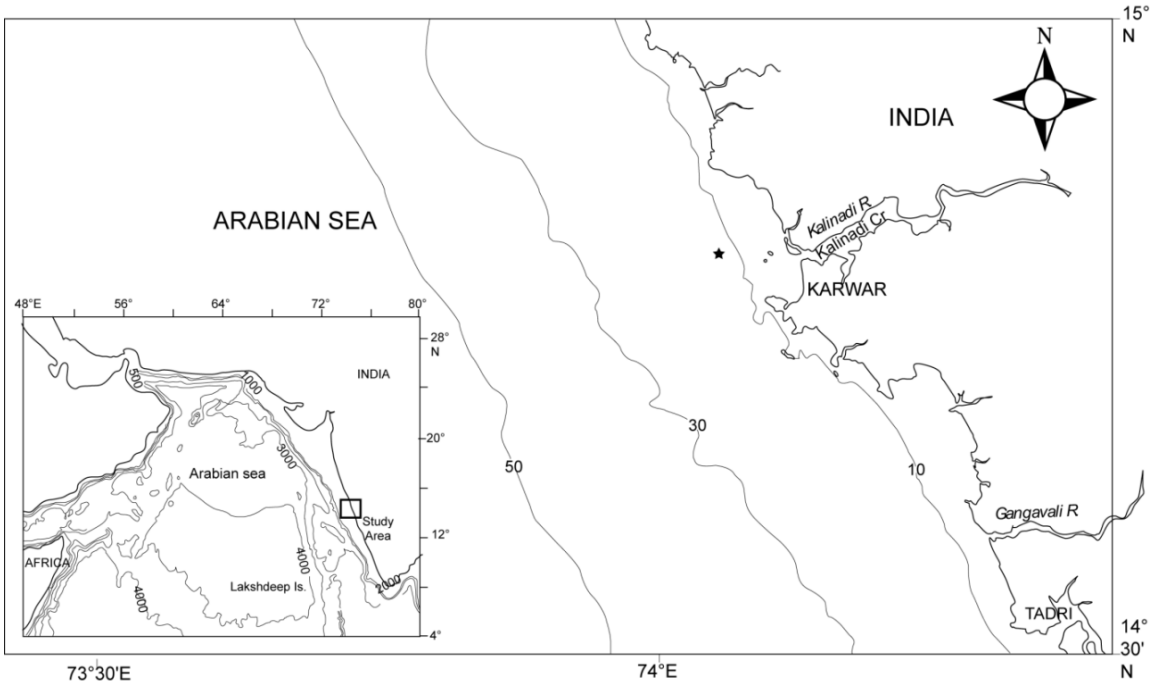

Figure 1. Study area along with the wave measurement location in eastern Arabian Sea

608
609

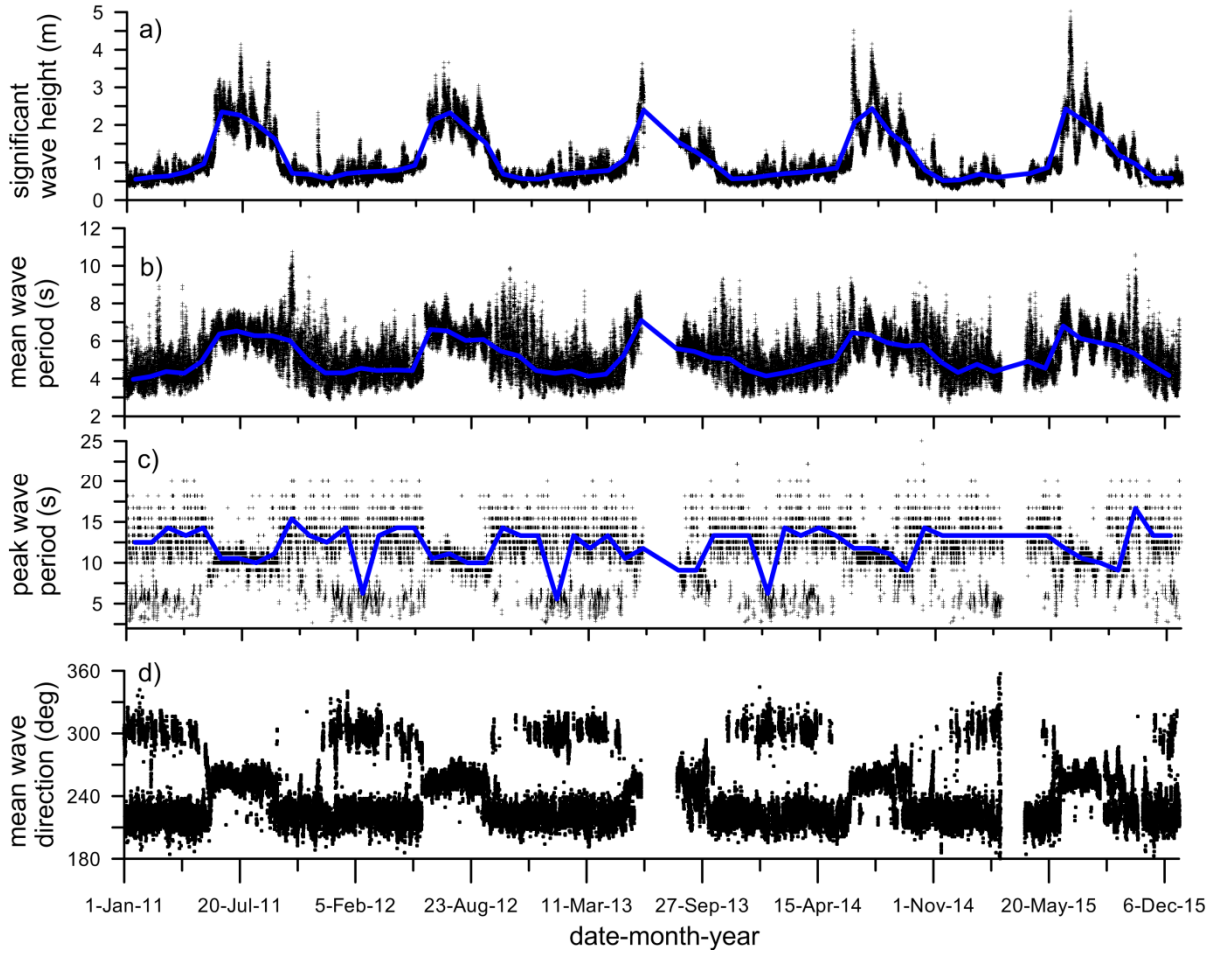

610
611 Figure 2. Time series plot of a) significant wave height, b) mean wave period, c) peak wave period
612 and d) mean wave direction from 1 January 2011 to 31 December 2015. Thick blue line indicates
613 the monthly average values
614

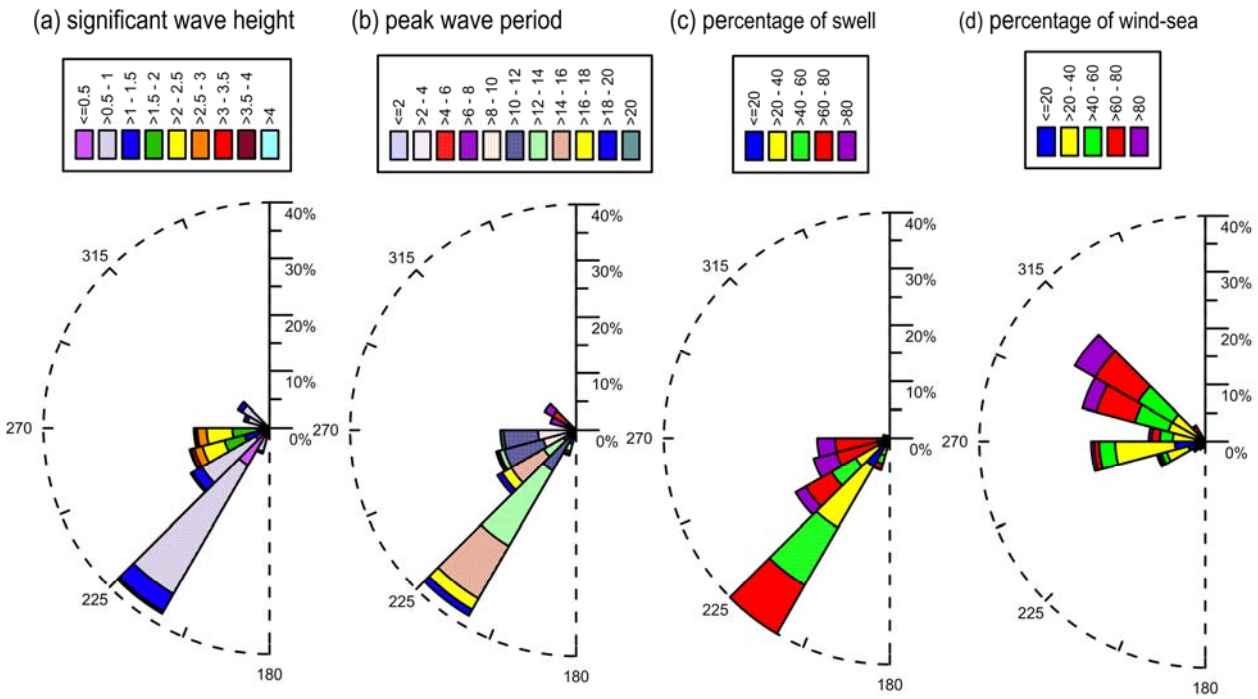

Figure 3. Wave roses during 2011-2015 (a) significant wave height and mean wave direction, (b) peak wave period and mean wave direction, (c) percentage of swell, (d) percentage of wind-sea and mean wave direction

620
621

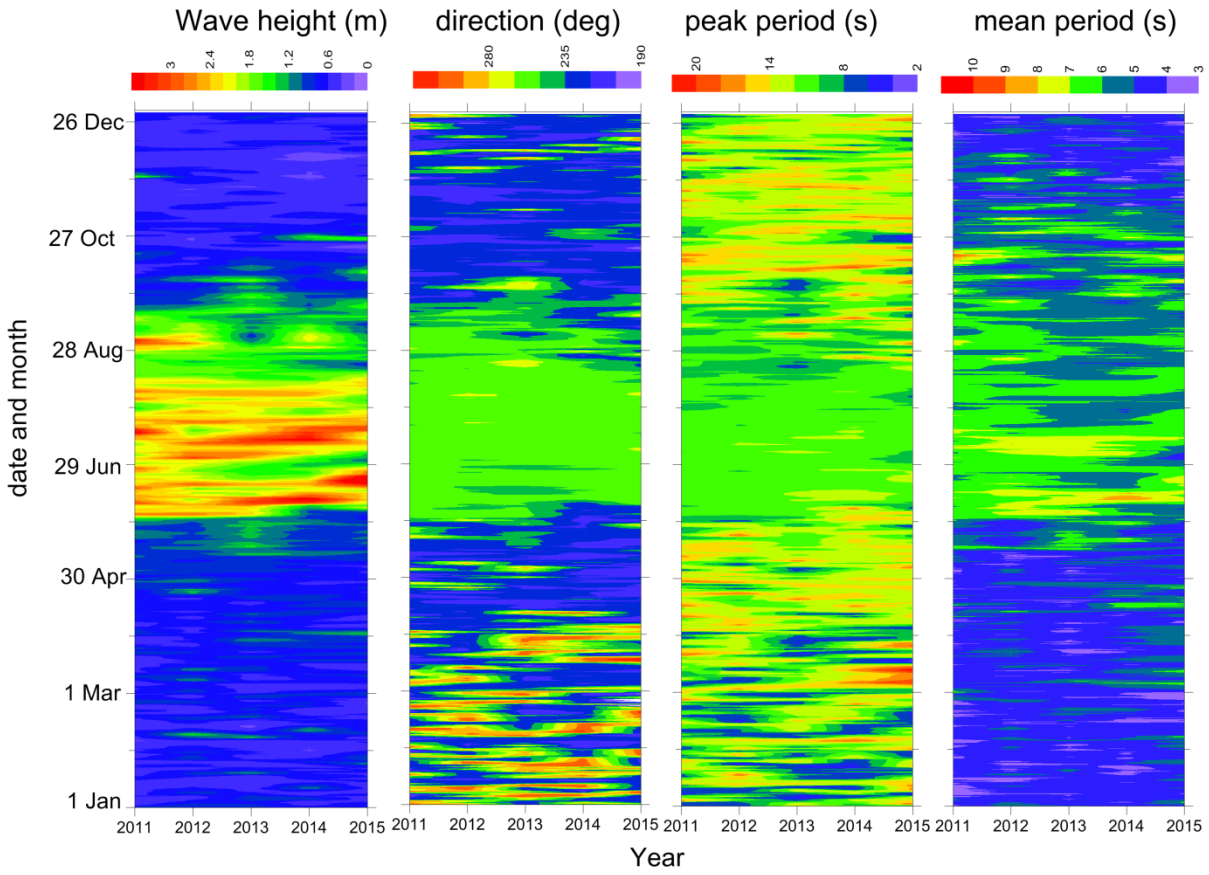

622
623 Figure 4. Date verses year plots of a) significant wave height b) mean wave direction, c) peak wave
624 period and d) mean wave period.
625

626
627
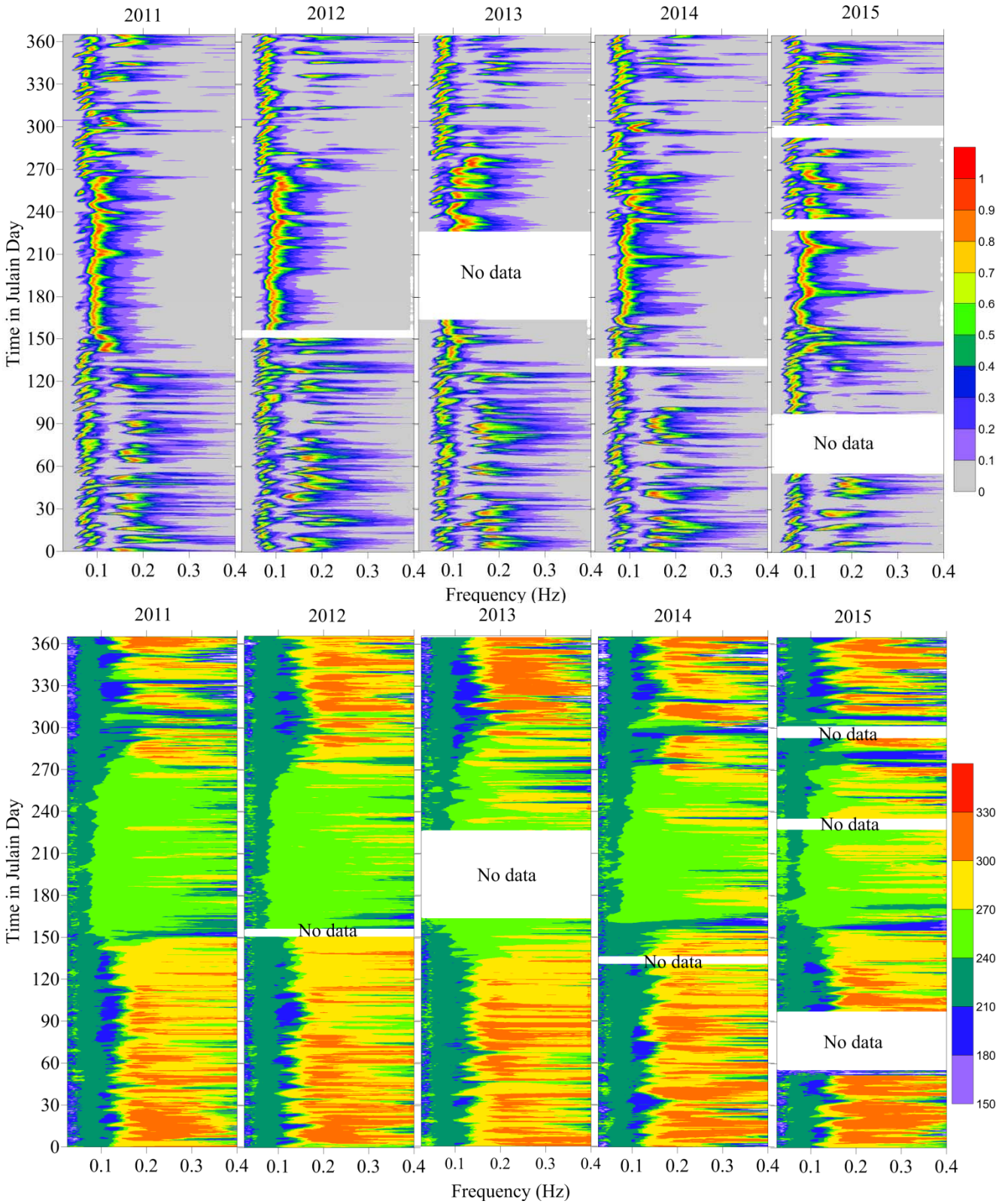

628
629
630 Figure 5. Temporal variation of normalized spectral energy density (top panel) and mean wave
631 direction (bottom panel) with frequency in different years

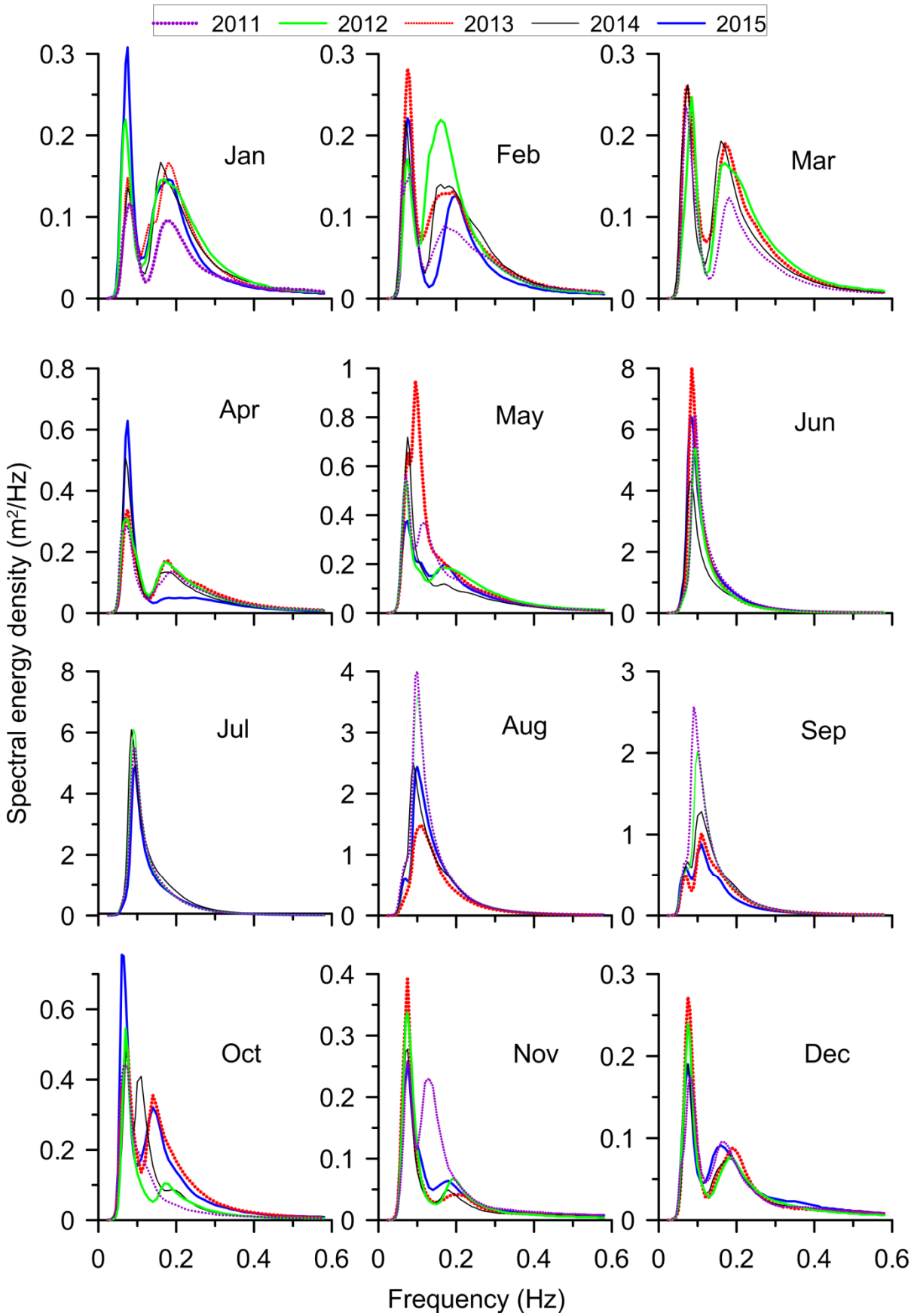

632
633 Figure 6. Monthly average wave spectra in 2011 to 2015

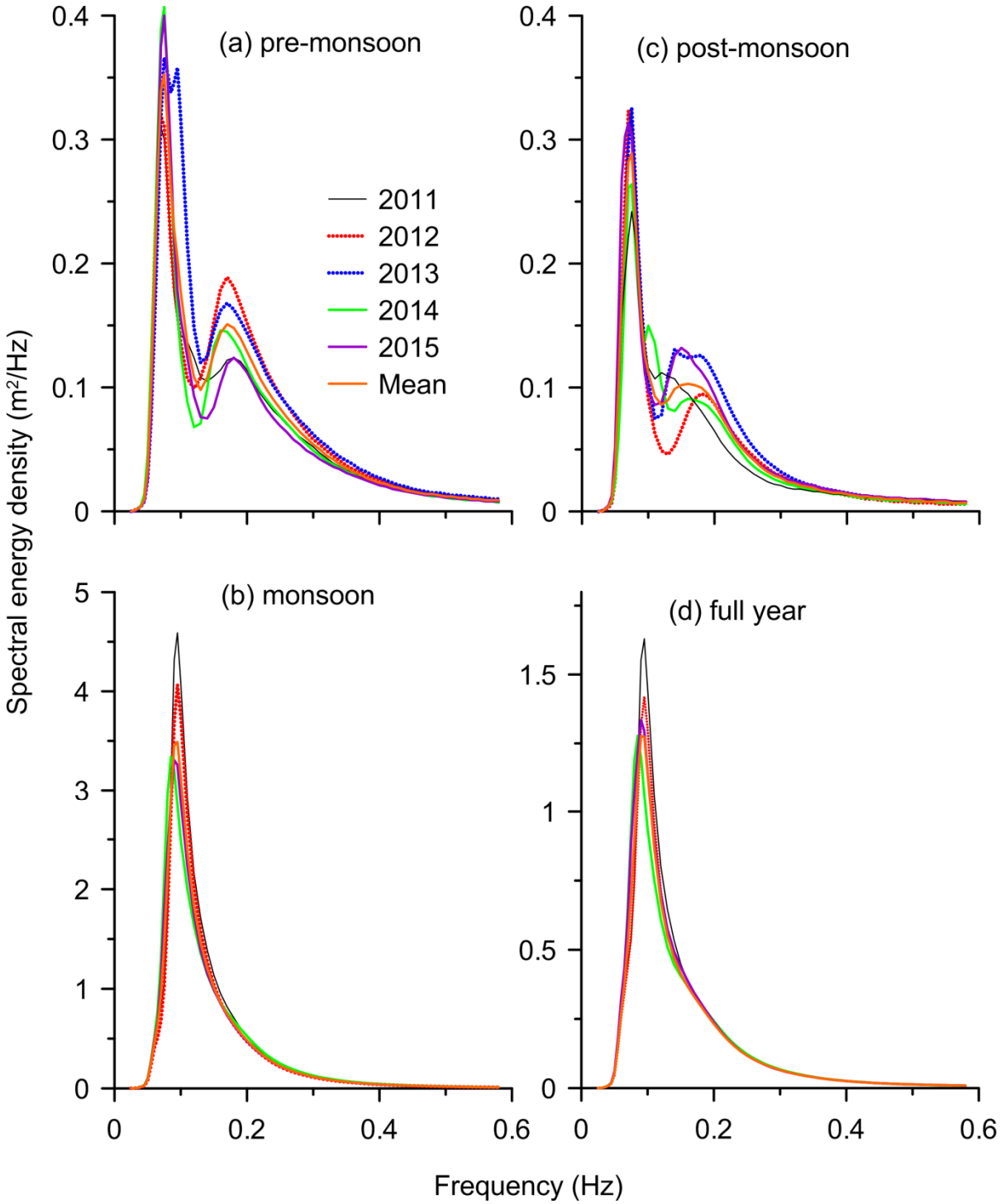

Figure 7. Wave spectra averaged over a) pre-monsoon (February-May), b) monsoon (June-September), c) post-monsoon (October-January) and d) full year in different years

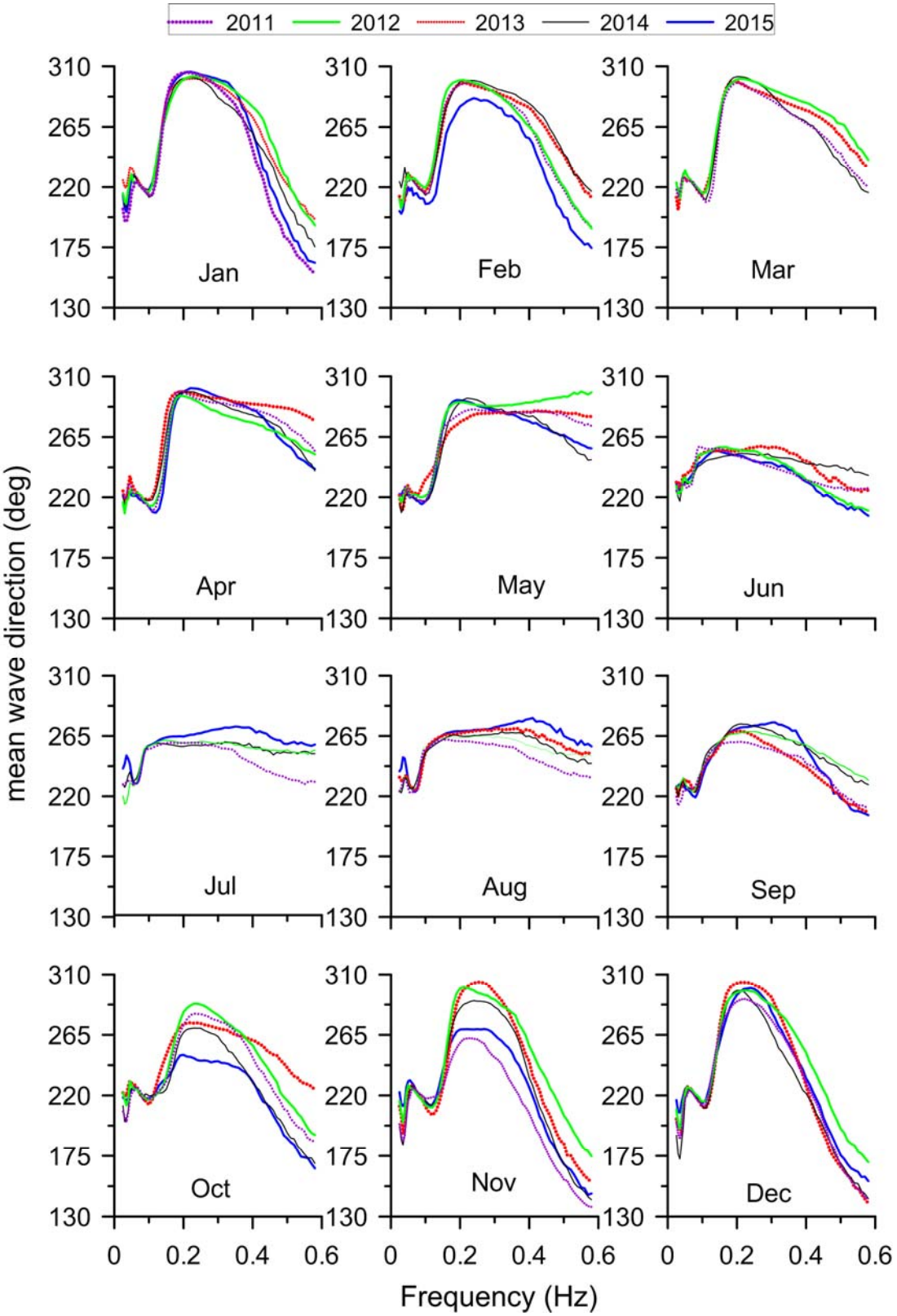

Figure 8. Monthly average wave direction at different frequencies in different months

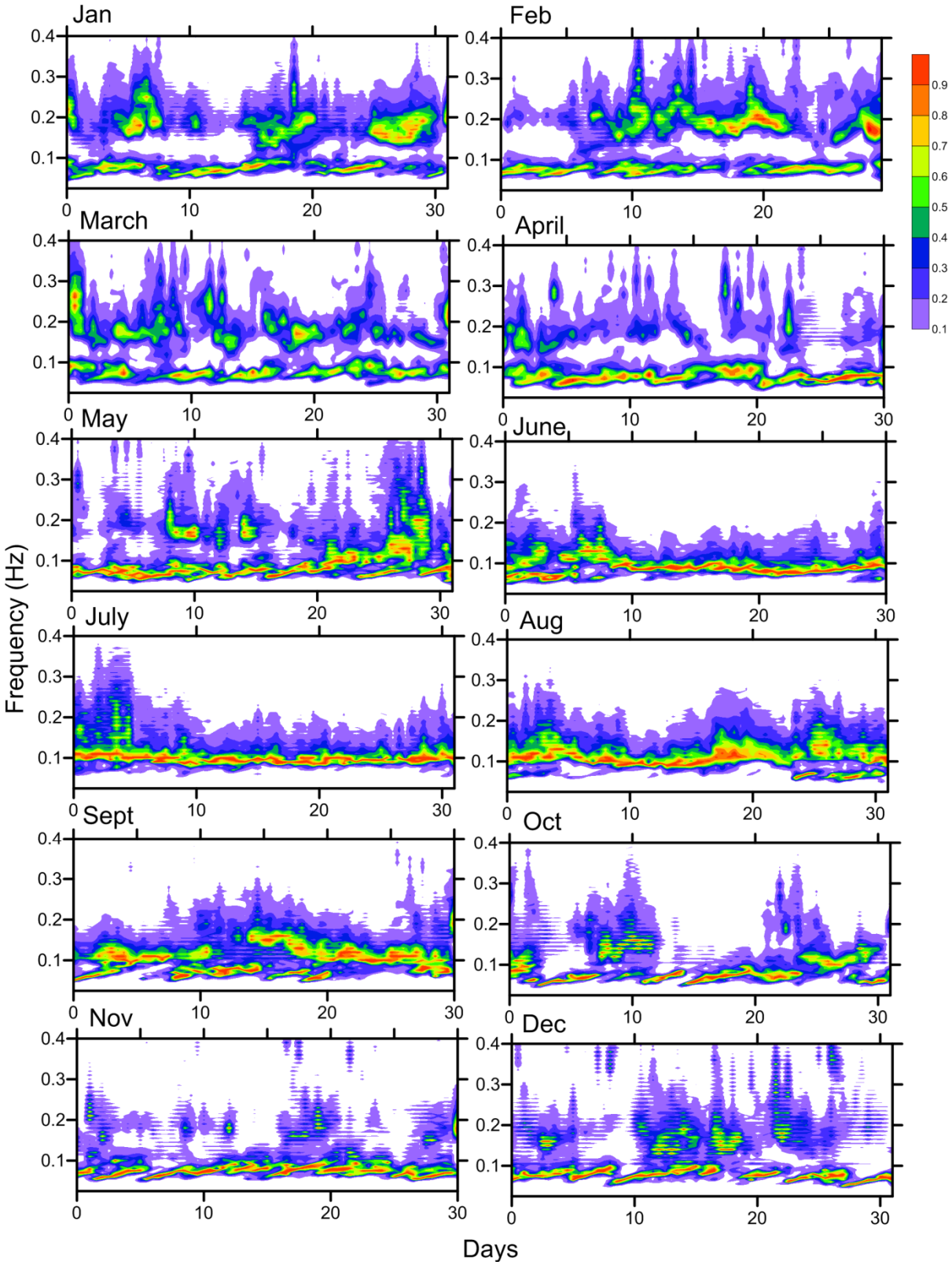

Figure 9. Temporal variation of normalized spectral energy density in different months (data from 2011 to 2015 used)

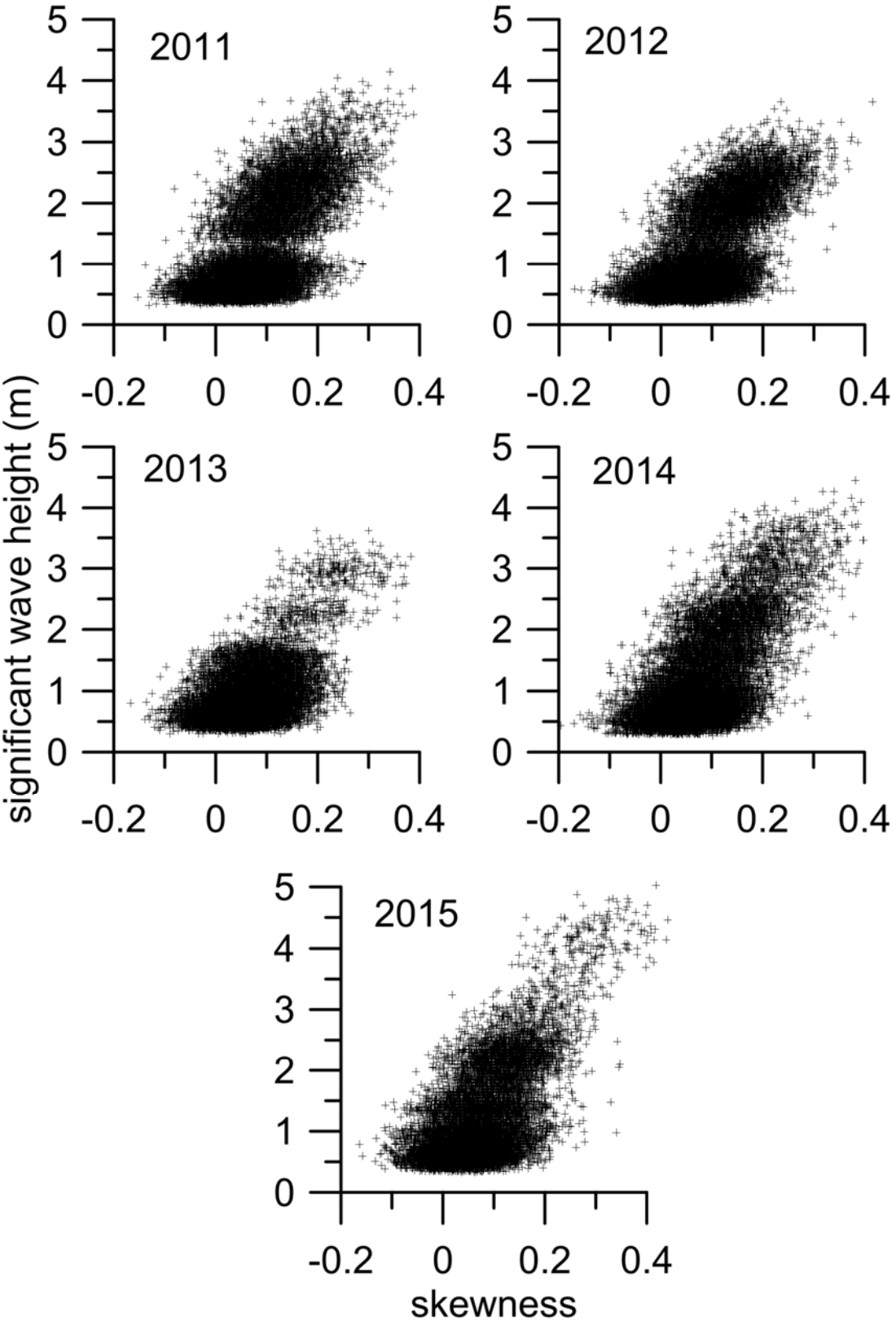

Figure 10. Scatter plot of significant wave height with skewness of the sea surface elevation in different years

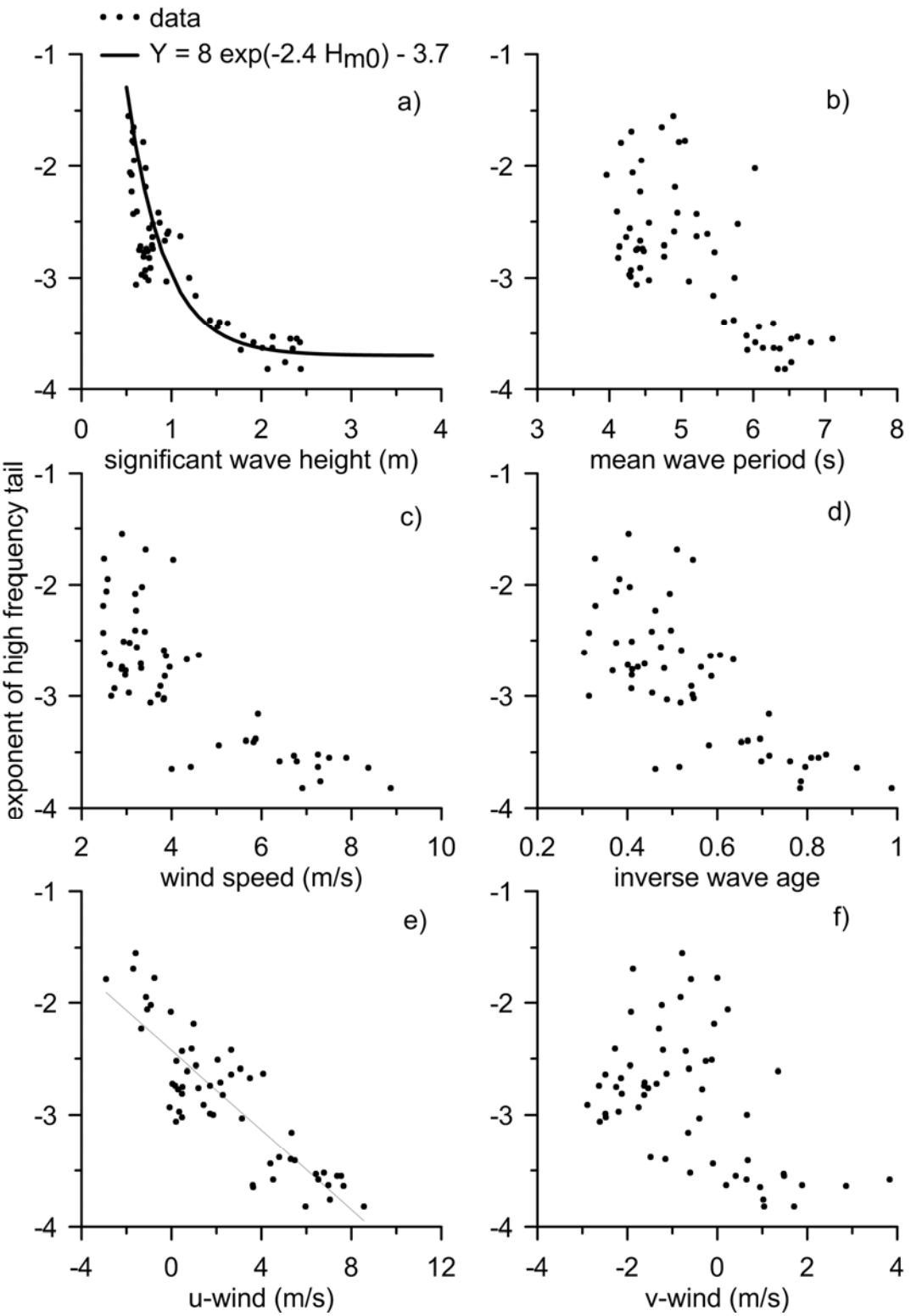

Figure 11. Plot of exponent of the high-frequency tail with a) significant wave height b) mean wave period, c) wind speed, d) inverse wave age, e) u-wind and f) v-wind

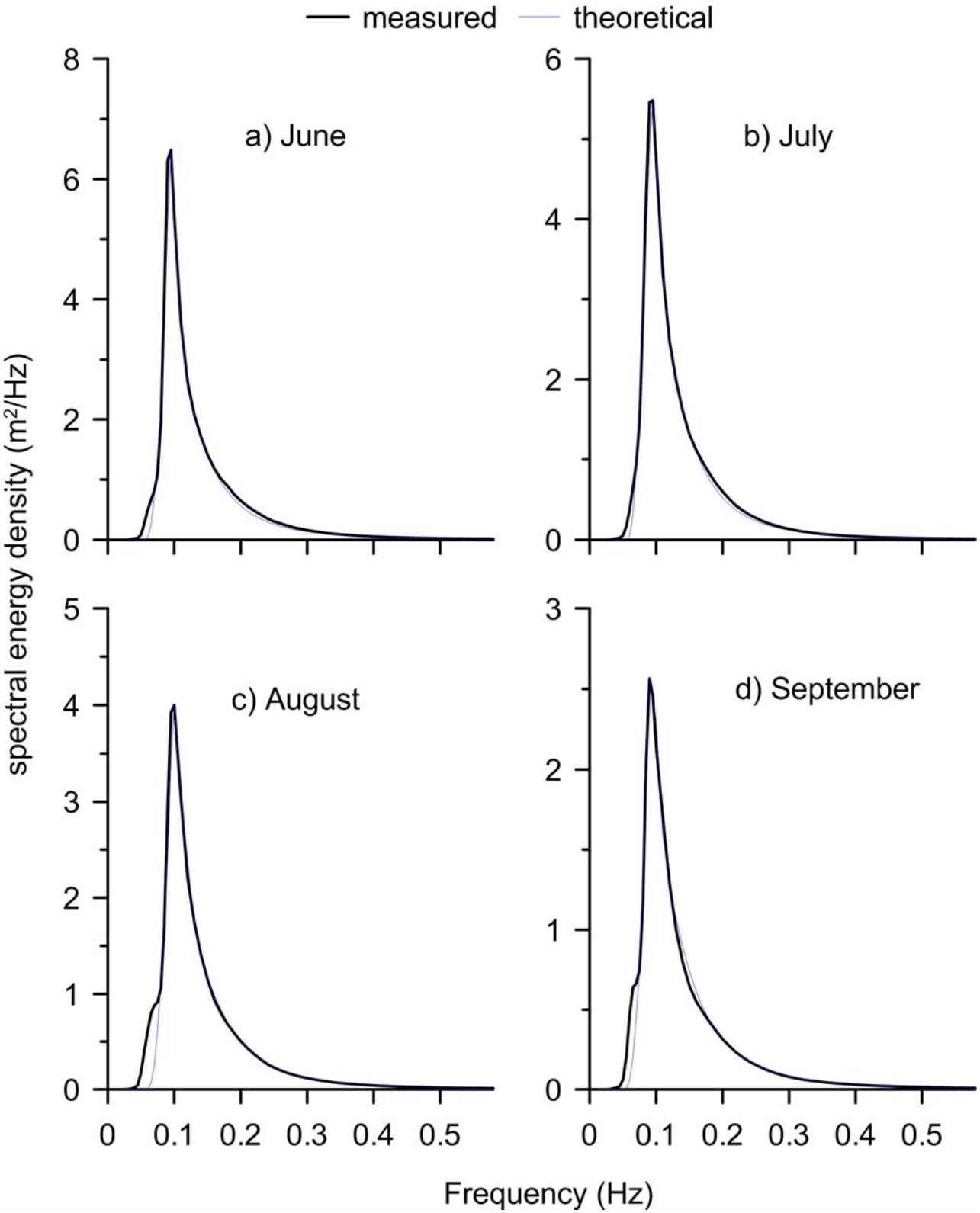

654
655 Figure 12. Fitted theoretical spectra along with the monthly average wave spectra for a) June, b)
656 July, c) August and d) September